


The Initial Distribution of Stars

Eli Walter Bressert

Submitted by Eli Walter Bressert to the University of Exeter as a thesis for the degree of Doctor of Philosophy in Physics, August, 2012.

This thesis is available for Library use on the understanding that it is copyright material and that no quotation from the thesis may be published without proper acknowledgement.

I certify that all material in this thesis which is not my own work has been identified and that no material has previously been submitted and approved for the award of a degree by this or any other University.

Signed: 

Mr Eli Walter Bressert

Date: ..06/08/2012...

Abstract

The primary focus of my PhD is to quantify the spatial distribution of star-forming environments from optical to radio wavelengths using data from the *Hubble Space Telescope*, the *Very Large Telescope*, the *Spitzer Space Telescope*, the *Herschel Space Observatory*, and the *Caltech Submillimeter Observatory*. Towards the end of my PhD study I have developed theoretical models. With these observational and theoretical avenues I have led a series of research projects to (1) quantify the initial spatial structure of pre-stellar cores and proto-stars, (2) test whether massive stars can form in isolation or not, (3) and develop a theoretical model on how young massive clusters form.

These research projects have been fruitful as my collaborators and I have shown that pre-stellar cores and stars form in a smooth continuum of surface densities from a few to thousands of stars per pc^2 . These two works have important implications on our understanding of what a young stellar cluster is and how star forming environments can evolve to form field star populations or gravitationally bound clusters. In my second study my collaborators and I found evidence for isolated massive star formation in the active star forming region 30 Doradus, in the Large Magellanic Cloud. The result impacts the field of the initial mass function and star formation models. Massive stars forming in isolation is consistent with a stochastically sampled initial mass function. Additionally, the result would put constraints on theoretical models on massive star formation. Continuing my work on massive star forming environments my collaborators and I have developed a theoretical model on how young massive clusters form. From the models we argue that feedback energies can be contained by the gravitational potential well of the massive progenitors. Furthermore, we predict the physical properties the massive cluster progenitors in terms of initial gas mass, radii and flux brightness to enable a search for these objects in Galactic plane surveys and upcoming telescopes. Using the common thread of spatial distribution analysis of star formation I describe my future research plans, which entails studies on extragalactic scales in the conclusion.

Contents

1	Introduction	14
1.1	Star formation: From gas to stars	14
1.2	Do all stars form in clusters?	15
1.3	Isolated massive star formation	17
1.4	Young massive cluster progenitors	18
1.5	Other works and research	19
1.6	Summary	21
2	The spatial distribution of young stars in the solar neighbourhood	22
2.1	Abstract	22
2.2	Introduction	22
2.3	Observations & Data	24
2.4	Σ_{YSO} Distributions	27
2.5	Results	27
2.6	Cluster Identification	29
2.7	Discussion and Conclusions	30
3	The spatial distribution of star formation in Perseus and Serpens	31
3.1	Abstract	31
3.2	Introduction	31
3.3	Observations & Analysis	32
3.3.1	<i>Herschel</i> Observations	32
3.3.2	Complementary IR surveys and YSO identifications	36
3.3.3	WISE	36
3.3.4	YSO identifications	36
3.4	Spatial distribution	36
3.4.1	Minimum spanning tree & clustering	37
3.4.2	Surface densities	39
3.5	Summary	40
3.6	Appendix	41
3.6.1	Intellimerge	41
3.6.2	WISE and c2d	43
3.6.3	Minimum Spanning Tree Extensions	44

4	Can massive stars form in isolation?	49
4.1	Abstract	49
4.2	Introduction	49
4.3	Observations	53
4.4	Method	56
4.4.1	Criteria	56
4.4.2	Spectral types & ages	58
4.5	Results	58
4.5.1	Local environment examples	62
4.5.2	Photometric completeness around the candidates	67
4.5.3	Binary detection probability	67
4.6	Discussion	69
4.6.1	Modeling potential underlying clusters	69
4.6.2	Comparing Monte Carlo simulations to observations	73
4.6.3	Mass & age discrepancies	74
4.6.4	Filamentary structures in 30 Doradus	75
4.6.5	Bow-shocks and the ISM in 30 Doradus	76
4.6.6	Number of isolated stars	77
4.7	Summary and Implications	77
4.8	Appendix	79
4.8.1	Hubble archival data	79
4.8.2	Probability test for chance alignment of runaway stars with filaments	79
5	How to find young massive cluster progenitors	82
5.1	Abstract	82
5.2	Introduction	82
5.3	Young Massive Cluster Formation	83
5.3.1	Initial conditions	83
5.3.2	Ionizing feedback, pressure, and star formation	84
5.4	Predicting Observed Proto-cluster Properties	85
5.4.1	Proto-cluster geometries	85
5.4.2	Prediction and observations	86
5.5	Discussion and Summary	88
6	Conclusions	90
6.1	Future research	92
6.1.1	Analysis & science impact	93
6.1.2	Research plan	93
6.1.3	Pilot Study: The most extreme Galactic protocluster	95

List of Figures

- 2.1 **Top panel:** The surface density distribution of the total sample of YSOs in the solar neighbourhood used in this work (black). A lognormal function with a peak at ~ 22 YSOs/pc² and a dispersion $\sigma_{\log_{10}\Sigma} = 0.85$ is shown as a dashed (red) line. **Bottom panel:** The same as the top panel but now broken into the three respective surveys. Note that Orion dominates the number statistics. 25
- 2.2 **(a)** The cumulative fraction of surface densities for the GB+Taurus, c2d, and Orion surveys. Each SF region included in the distributions has $N(\text{YSOs}) \geq 10$ and a sufficient field-of-view to properly calculate stellar surface densities. The Orion survey stops at 73% for the cumulative fraction since the ONC is excluded. We adopt a 65% disk fraction for all of the SF regions. We normalised each curve by the number of YSOs in each survey. **(b)** With the GB+Taurus, c2d, and Orion surveys combined we see Class I & II distributions having similar profiles with a small offset in density, showing that we are likely seeing the primordial distribution of the YSOs. **(c)** With all of the *Spitzer* surveys combined we compare several cluster definitions. The vertical grey lines from left to right are Lada & Lada (2003), Megeath et al. (in prep.), Jørgensen et al. (2008), Carpenter (2000), and Gutermuth et al. (2009) stellar density requirements for clusters. These values correspond to 3, 10, 20, 32, and 60 YSOs pc⁻² and intersect the corrected cumulative distribution profile, implying that 87%, 73%, 62%, 55%, and 43% of stars form in clusters, respectively. The percentages correlate to what fraction of stars form in “clusters” based on the various definitions. The black vertical line is for a dense cluster where $\Sigma \geq 200$ YSOs/pc². The fraction of YSOs in a dense cluster is < 26%. 28
- 3.1 **[Left]** *Herschel* 350 μm image of Perseus-W. The well-known subregions (NGC 1333, B1, L1448, L1451, and L1455) are marked with black circles and labelled. **[Right]** Respectively, the YSO minimal spanning tree is shown using light blue and black lines, which represent branch lengths that are shorter (black) or longer (blue) than the cutting length (see main text for details). Dense YSO groups are shown by the collections of coloured filled markers. The grey triangles are the cores and their groups are marked by the light green convex hulls. The thick black line marks the region covered by the *Spitzer* c2d survey. 34

- 3.2 The Serpens 350 μm image from *Herschel*, with annotations/descriptions as per Fig. 3.1. 35
- 3.3 The surface densities (Σ) of the cores and YSO_{WISE} in western Perseus and Serpens combined. The red dotted line and the blue dashed line represents the cores and the YSO_{WISE}, respectively. The solid black line represents the combined cores and YSO_{WISE}. The light grey solid line is the profile shown in Bressert et al. (2010) for nearly all YSOs in the solar neighbourhood using several *Spitzer* Legacy surveys. The data is hinting that star formation at even the earliest stage is scale-free as stated in Bressert et al. (2010), but further analysis using more *Herschel* data for other star forming regions is needed. 39
- 3.4 Examples of photometry recovery with Intellimerge on three different sources. The letters *S*, *R*, and *N* stand for “standard”, “recovered” and “no detections”, respectively. Standard sources are the high confidence sources that are initially included in the master table. The recovered photometry are those that are found in the lower confidence photometry lists. In the upper panel, photometry is recovered in the 500 μm band for a source close to other bright sources. In the middle panel, photometry for a binary source well resolved at short wavelengths is recovered up to 350 μm . In the bottom panel, a source detected at high confidence at long wavelength is recovered at 250 μm , but no reliable photometry is possible at shorter wavelengths. 43
- 3.5 **[Left]** WISE identified YSOs in Perseus using the colour-colour space method (Koenig et al. 2012). The gold circles are Class I sources and the red circles are Class II sources. The light gray sources are diskless stars in the same field-of-view where the YSOs are identified. **[Right]** WISE identified YSOs in Serpens with the same colour scheme described for Perseus. 44
- 3.6 The intersection point between the two solid lines is a result of to least-square fits, which is how the critical branch length is determined. The left-hand least-squares fit is based on the data from the left to right and the right-hand least-squares fit is based on the data from right to left. The intersection point that represents an *x* and *y* maximum is then selected as the critical branch length. 45
- 3.7 MST branch length for Perseus and Serpens, where the red markers (+) represent the WISE YSOs and the blue markers (\times) represent the cores. The black markers (\bullet) are the branch lengths from the c2d YSO population. The blue and red vertical lines represent the critical branch cutting lengths for the cores and the YSO_{WISE}, respectively. In the case of Perseus, we implemented a two-step MST group identification algorithm. The first cutting length for the YSO_{WISE} in Perseus identifies NGC 1333 (solid red line). The second cutting length identifies the remaining MST groups in the western Perseus region (dashed red line). See the appendix for further details on how the algorithm works. 46

- 4.1 The 16 candidates, isolated massive stars, in 30 Doradus are marked with red circles. Figs. 4.5–4.9 show sub-fields of this region to highlight gas/dust filamentary structures that are likely to be associated with the massive stars in question. The stars are identified with the numbers used for the VLT FLAMES Tarantula Survey. 54
- 4.2 2.5×2.5 parsec (10''×10'') logarithmically stretched grey scale images of each of the stars. All of the candidates were observed in the F814W band except for VFTS 682 and VFTS 849, which are observed in the F673N and F606W bands, respectively. Additionally, all of the candidates were observed with the WFPC2, except for VFTS 123, 208 and 216 which were observed with ACS. 57
- 4.3 The 90% completeness magnitude limit as a function of radius for VFTS 385 (using HST/WFPC2). The closest detectable source to the candidate is ~ 0.15 pc, where the upturn begins. VFTS 385 is the brightest observed candidate presented in this paper. 60
- 4.4 HST stellar surface density distributions (cumulative - see Lamb et al. 2010) around VFTS 208. The black line with triangles is the HST F555W band and the blue line with circles is the HST F814W band. Due to the saturation on the ACS images caused by the candidate (candidate reference point is at 0 pc), VFTS 208 represents a worst case. However, even here we see that there is no stellar count increase from 3 pc and inwards (to 0 pc) toward the candidate. This has been observed similarly for each candidate. 63
- 4.5 Filamentary structures possibly associated with the four candidates: VFTS 385, 398, 470 and 581 (red circles). The background image is from the VLT HAWK-I K_s band and the four subplots on the right are K_s , $70 \mu\text{m}$, $70 \mu\text{m}$ and $\text{H}\alpha/\text{H}\beta$ (Lazendic et al. 2003) mps for VFTS 385, 398, 470 and 581, respectively. The black boxes in the main image correspond to the field-of-view for the subplots on the right, where the $70 \mu\text{m}$ subplots are larger due to their lower resolution. Different stretches are used to highlight the filamentary associations in the subplots. 64
- 4.6 V-band optical image with $70\mu\text{m}$ contours from *Spitzer* overlaid, in the region of VFTS 208 and 216. The stars are associated with a large filament extending southeast from the direction of NGC 2060. The radial velocities of both stars agree to within 5 km s^{-1} . VFTS 216 may be related with a bow shock (see Fig. 4.7). 65
- 4.7 VFTS 216 (left target) may possibly be related to a bow shock as seen above. The image is a $24 \mu\text{m}$ map from the SAGE Survey. If the O-star is indeed related to the bow shock, then its candidacy is ruled out as an isolated massive star. At the distance of the LMC, the bow shock is estimated to be 5 pc across. 66
- 4.8 VFTS 488 is shown in the $70 \mu\text{m}$ map as a red dot (main) and K_s as a red circle (subset). The red box in the $70 \mu\text{m}$ map represents the subset image's field-of-view. VFTS 488 is associated with a filament in $70 \mu\text{m}$ and the K_s subset image shows that it's located in a relatively sparse field of stars. 69

- 4.9 VFTS 706 is shown in the $70 \mu\text{m}$ map (main) and K_s (subset). The red box in the $70 \mu\text{m}$ map represents the subset image's field-of-view. The candidate is located in a region of high $70 \mu\text{m}$ emission, where filaments appear to be in the peripheral region. This is similarly seen in the subset where ionised material is near the candidate. 70
- 4.10 VFTS 682, a Wolf-Rayet star that is discussed in further detail by Bestenlehner et al. (2011), is shown in the K_s band (main) marked by a red circle and $H\alpha/H\beta$ derived map as a red dot (subset). The red box in the K_s image represents the subset image's field-of-view. The candidate is located in a relatively sparse field of stars and the subset shows that's located in a region of relatively high A_V . VFTS 682 is the most massive candidate presented in this paper. 71
- 4.11 From left to right, the $5\times 5 \text{ pc}$ ($20''\times 20''$) images of the simulated *MASSCLEAN* clusters of 420, 1000, and $4000 M_\odot$. The images were made of simulated clusters, with HST ACS resolution, at the distance of the LMC in the V-band. The green diamonds mark the brightest/most massive star in the cluster. The red circles indicate stars that would have been detected on the actual images (see Fig. 4.3). In all cases, the underlying cluster would have been detected. 74
- 4.12 [From left to right] The expected number of observable stars associated with a 25, 40, and $100 M_\odot$ massive star in 420, 1000, and $4000 M_\odot$ clusters, respectively based on the 30,000 Monte Carlo simulation runs. The black solid lines are the mean number of stars per mass bin and the dashed red lines are the 1σ dispersion. Stars with masses below $3 M_\odot$ are greyed out on the left hand side of the plot, as those to the right of it are observable. The expected number of observable stars with a 1σ dispersion from the mean are 11, 53, and 148 assuming $A_V \sim 1$. According to the estimated number of excess stars for the candidates (see Table 4.3) we should have detected such cluster presence around the $25 M_\odot$ candidates at minimum. 74
- 4.13 A diagram showing how the probabilistic method should be conceptualised. The radius $R = R_{\text{boundary}} - R_{\text{cluster}}$. All the stars outside of the cluster are initially assumed to be runaways for the binomial probability problem to calculate the likelihood of multiple alignment events between the runaways and the filaments (grey clouds). The filaments at these scales, $> 5 \text{ pc}$, will not be affected by a single O-star such that nothing remains. 81

- 5.1 The mass-radius parameter-space for clumps partitioned by radii for r_Ω (solid blue) and r_{vir} (solid black). MPC candidates are defined with the following properties (green shaded region): a minimum mass of $3 \times 10^4 M_\odot$, $< r_\Omega$ for the $\leq 8.4 \times 10^4 M_\odot$, and r_{vir} for $> 8.4 \times 10^4 M_\odot$. Clump masses and sizes are plotted on top from three different data catalogs: IRDCs (Rathborne et al. 2006), HOPS clumps (Walsh et al. 2011), and YMCs (Portegies Zwart et al. 2010). The YMCs are converted to their possible clump progenitors by assuming that SFE is $\sim 30\%$, which boosts the mass of the systems by a factor of 10/3. The scaled YMC progenitors happen to lie near the critical r_Ω line without any tweaking of parameters. Two published sources that have radii less than both their respective r_Ω and r_{vir} are G0.253+0.016 (L12; Longmore et al. 2012) and an *extragalactic* massive proto-cluster candidate reported in Herrera et al. (H12; 2012). The MPC candidates reported in Ginsburg et al. (GS; 2012) are shown as squares. 88
- 6.1 Radius versus mass for Galactic dense, cluster-forming molecular clouds. The typical properties of Galactic open clusters, young massive clusters, and globular clusters are marked by the shaded polygons. Plus symbols show ammonia clouds detected in HOPS (blue/brown denote an assumed near/far kinematic distance, respectively). Green crosses show infrared dark clouds (IRDCs) from the survey of Rathborne et al. (2006). The hatched rectangles show the mass-radius range of different stellar clusters (see Portegies Zwart et al. 2010). The black dots show Galactic young massive clusters. G0.254+0.016 is marked with a red star and clearly stands out as unique. It has a mass and radius that would be expected of a molecular cloud progenitor of a large YMC or a globular cluster. 96
- 6.2 Simulations of a massive ($10^4 M_\odot$, 1 pc) proto-cluster using two different density distributions: centrally condensed (upper panels) and hierarchical fragmentation (lower panels). The black contours represent what the ALMA Early Science observations (e.g. the pilot study mentioned above) would be able to detect at the same distance as G0.254+0.016 (~ 7 kpc) at 90 GHz in the extended configuration. We will be able to determine whether hierarchical structure is present or not in these proto-YMCs and if such structure is present we will be able to quantify it using a method devised by Lomax et al. (2011). ALMA's performance in angular resolution and dynamic range will only improve as time progresses, enabling us to (1) observe proto-YMC candidates at further distances and (2) survey a large number of the candidates in a short amount of time. 97

List of Tables

2.1	The <i>Spitzer</i> surveys used in the present work includes 12 star forming regions with 3857 YSOs. The numbers in brackets refer to the total number of sources in the catalogues for each region, while the number before the brackets is the number used in the present analysis. The difference is due to the application of the absolute magnitude cuts as well as the elimination of class III YSOs from the sample. The sources for these SF regions are the 1) GB survey, 2) c2d survey, 3) Orion survey and 4) Taurus survey.	23
3.1	Source detections of the YSOs and cores.	37
3.2	Source statistics of the YSO _{c2d+WISE} Class I and Class II objects, denoted as CI and CII respectively, and the cores.	37
3.3	MST identified groups in Perseus-W and Serpens (denoted with P- or S- in the <i>Association column</i>). <i>Herschel</i> detected cores are denoted as HC. The YSO groups presented here only come from the WISE catalogue.	48
4.1	The 16 candidates that most likely formed in isolation.	61
4.2	Average binary detection rates.	68
4.3	Number of stars around each candidate based on observations and Monte Carlo stellar cluster simulations.	73
4.4	Comparison of candidate masses using both evolutionary models with isochrones and Weidner & Vink (2010) models.	75
4.5	The details of the HST data used in this paper.	79
5.1	Predicted Proto-cluster Properties	89

Declaration

This thesis contains work published or pending publication as papers. The results of Chapter 2 has been published in the Monthly Notices of the Royal Astronomical Society (MNRAS), volume 409, pp. 54. The results of Chapter 3 has been submitted to the Astronomy & Astrophysics (A&A) journal and is pending for publication. Chapter 4 has been published in the A&A, volume 542, pp. A49. Chapter 5 has been accepted for publication in the Astrophysical Journal.